Transport Economics and Management 3 (2025) 391–402

Contents lists available at ScienceDirect

Transport Economics and Management

journal homepage: www.journals.elsevier.com/transport-economics-and-management

Exploring the effects of space weather-caused satellite navigation failure on fuel consumption and aircraft emissions: A simulated study

Dabin Xue [a,b,c], Yifan Xu [d], Shiwei Yu [e], Zhizhao Liu [f,g,*]

[a] Department of Land Surveying and Geo-Informatics, The Hong Kong Polytechnic University, Hong Kong, China
[b] State Key Laboratory of Solar Activity and Space Weather, National Space Science Center, Chinese Academy of Sciences, Beijing, China
[c] School of Aviation, University of New South Wales Sydney, Kensington, Australia
[d] College of Civil Aviation, Nanjing University of Aeronautics and Astronautics, Nanjing, China
[e] Department of Civil and Environmental Engineering, The Hong Kong University of Science and Technology, Hong Kong, China
[f] State Key Laboratory of Climate Resilience for Coastal Cities, Department of Land Surveying & Geo-Informatics (LSGI), The Hong Kong Polytechnic University, Hong Kong, China
[g] Meteorological Observation Center, China Meteorological Administration (CMA), Beijing, China

ARTICLE INFO

Keywords:
Satellite navigation failure
Fuel consumption
Aircraft emissions
Flight route design
Economic loss

ABSTRACT

Satellite navigation provides aircraft with precise positioning and navigation services. However, space weather can induce ionospheric irregularities and elevate the total electron content in the ionosphere, causing satellite navigation failure. Consequently, aircraft will navigate using ground aids and be disabled to fly along Great Circle Routes, increasing flight distance, fuel consumption, and aircraft emissions. To explore the effects of satellite navigation failure on flight operation, this study simulates satellite navigation failure scenarios and proposes Air Traffic Management (ATM) solutions. Specifically, the first step designs the ground aid-based shortest path using the Dijkstra algorithm, followed by the calculations of fuel consumption and aircraft emissions using the Base of Aircraft Data (BADA) and the aircraft Engine Emissions Databank (EEDB), respectively. Based on the collected 11,037 U.S. flight plans on 5 February 2024 (UTC), simulations show that a single-day satellite navigation failure can result in an increase of flight distances by 2,371,777 km, fuel consumption of 7176 tons, and CO_2 emission of 22,604 tons. While this study focuses on simulations in the U.S., the findings have a broad implication and can serve as a framework to address space weather effects on aviation in other regions of the world.

1. Introduction

Satellite navigation, based on the Global Navigation Satellite System (GNSS), is a foundational technology in modern aviation, offering global positioning services with unparalleled accuracy and reliability [1]. This capability enables closer aircraft spacing without compromising safety, thus enhancing airspace capacity and flight efficiency [2]. In addition, aircraft can fly directly between any two points along the Great Circle Routes (GCR) instead of flying along waypoints, reducing flight times and fuel consumption [3]. Moreover, even in remote or oceanic regions lacking traditional ground-based navigation aids, the positions of aircraft can be easily determined.

However, space weather, primarily driven by solar activities, can significantly impact satellite navigation systems, posing a high risk to their reliability and performance [4,5]. One of the primary effects of space weather on satellite navigation is the disruption of radio signals used for precise positioning and navigation [6,7]. Solar flares and Coronal Mass Ejections (CMEs) can release intense bursts of radiation and charged particles [8], which interfere with the signals transmitted from satellites to receivers on Earth [9]. This interference can lead to signal degradation [10], increased noise levels [11], and even complete signal loss [12], compromising the accuracy and availability of satellite navigation services. Magnetic storms, another consequence of space weather events, can disrupt the Earth's magnetic field [13,14] and induce fluctuations in the ionosphere [15,16], the upper region of the Earth's atmosphere where satellite signals propagate [17,18]. These disturbances can cause signal bending, delay, and scintillation, affecting the quality of satellite navigation signals received by users [19]. In severe cases,

* Corresponding author at: State Key Laboratory of Climate Resilience for Coastal Cities, Department of Land Surveying & Geo-Informatics (LSGI), The Hong Kong Polytechnic University, Hong Kong, China.
E-mail address: george.liu@polyu.edu.hk (Z. Liu).

https://doi.org/10.1016/j.team.2025.10.001
Received 21 July 2025; Received in revised form 29 September 2025; Accepted 9 October 2025
Available online 11 October 2025

magnetic storms can lead to ionospheric irregularities and increase the Total Electron Content (TEC) in the ionosphere [20,21]. As a result, satellite navigation systems may experience degraded performance or become temporarily unusable during intense geomagnetic activities. Furthermore, space weather events can ruin the overall integrity and availability of satellite navigation systems by causing anomalies in satellite operations and infrastructure [22]. Solar radiation can damage satellite electronics, solar panels, and other critical components, leading to temporary malfunctions or permanent failures [23]. Besides, Solar Energetic Particles (SEPs) from solar events can degrade the atomic clocks onboard satellites, affecting the timing accuracy essential for precise positioning [24]. A comprehensive summary of space physics can be found in [25]. Fig. 1 shows the schematic diagram of normal GNSS signals and disrupted GNSS signals.

In the event of satellite navigation failure, the navigation mode of aircraft has to shift to ground-based navigation, relying on VHF Omni-directional Range (VOR), Distance Measuring Equipment (DME), and Non-Directional Beacon (NDB) [26]. This could decrease airspace capacity and disrupt the balance between flight demand and airport capacity, necessitating flight rescheduling or cancellations. In prior studies, Xue et al. [27] conducted simulations using forecasted flight data for Hong Kong International Airport in 2030 to examine the impacts of satellite navigation failures on various flight parameters, including cancellations, ground delays, airborne delays, and flight diversions, estimating economic losses for a single event between €3.18 million and €4.18 million depending on the lead time of the forecasted failure. Xue et al. [28] further analyzed the effects of the 2003 Halloween storm on the top 50 busiest airports in the Continental United States, estimating economic costs of €2.43 million associated with Area Navigation (RNAV) and Continuous Descent Approach (CDA) failures during the 2003 Halloween storm. In a subsequent study, Xue et al. [29] projected flight volumes for the Greater Bay Area (GBA) of China in 2025 and found that a single satellite navigation failure could incur tens of millions of Euros in economic costs, depending on the failure duration and the timing of ground navigation-based landings.

While previous studies primarily focused on aircraft navigation in the terminal area, particularly in the aircraft landing or approaching phases, this study shifts the attention to the effects of satellite navigation failure during the cruising phase, with a specific emphasis on fuel consumption and aircraft emission considerations. The workflow of this study is as follows. First, the shortest path from the cursing starting point to the cursing ending point is designed using the Dijkstra algorithm based on the geographical locations of ground navigation aids. Then, fuel consumption is calculated based on the Base of Aircraft Data (BADA) considering wind effects, followed by the calculations of aircraft emissions based on the aircraft Engine Emissions Databank (EEDB). Analyzing 11,037 U.S. flight plans on 5 February 2024, simulation findings demonstrate that a one-day satellite navigation failure can increase flight distances by 2,371,777 km, necessitating an extra consumption of 7176 tons of fuel and leading to corresponding increases in aircraft emissions, e.g., 22,604 tons of CO_2. Furthermore, this study examines the economic losses of various Air Traffic Management (ATM) strategies, including flight canceling, rescheduling, and rerouting. It can be concluded that in certain scenarios, flight rescheduling can lead to the lowest economic losses, making it a viable alternative strategy in addressing satellite navigation failures, whereas flight cancellation always appears less justifiable. Statistically, solar activity has an 11-year cycle [30,31], and we believe that this study can serve as guidance for aviation operations to make contingency plans for future space weather-caused satellite navigation failure scenarios.

The rest of this study is structured as follows: **Section 2** examines the effects of the Halloween storm on satellite navigation through historical analysis. **Section 3** outlines the relevant models used for flight route design, fuel consumption calculation, and aircraft emissions estimation. **Section 4** provides a description of the flight data and the accompanying wind information in the U.S. **Section 5** presents the simulated results regarding the consequences of satellite navigation failure. The broader implications and a critical discussion of these results are provided in **Section 6**. Finally, **Section 7** concludes the study by summarizing the key findings and offering final remarks.

2. Halloween storm effects on satellite navigation

GNSS operates on the principle of mathematical trilateration, and the accuracy of GNSS positioning relies on various factors, including satellite clock error, satellite orbit error, ionospheric delay error, tropospheric delay error, receiver noise error, and multipath error. Among these, ionospheric delay error is particularly significant, with potential errors ranging from a few meters to tens or even hundreds of meters. As GNSS signals traverse the ionosphere, the propagation is adversely affected by the density of electrons and ionized particles in the atmosphere, collectively degrading the performance of satellite-based positioning and navigation. The ionospheric delay error ($\Delta\rho_I$) negatively correlates with TEC along the signal propagation path and is inversely proportionate to the square of the radio frequency f, expressed below:

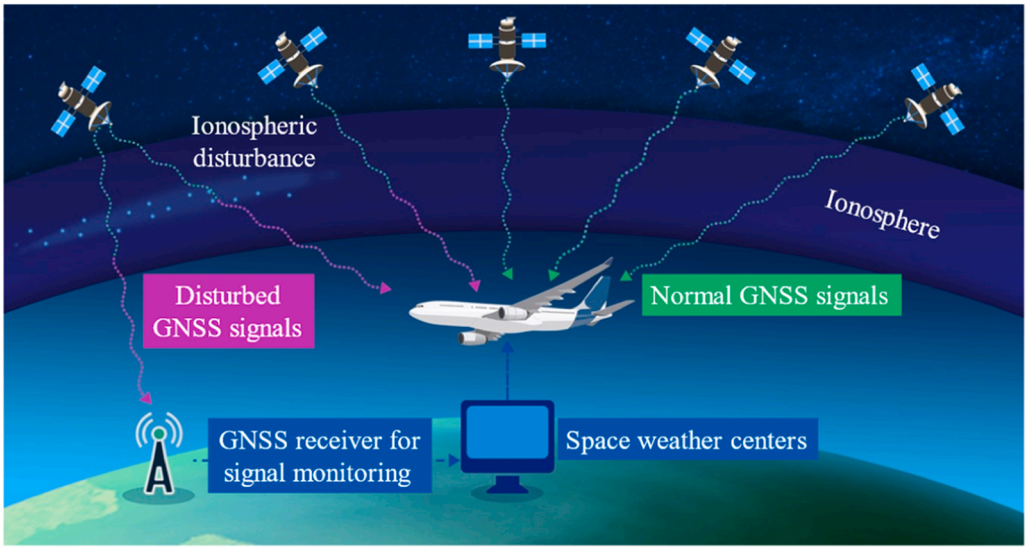

Fig. 1. Schematic diagram of normal GNSS signals and disrupted GNSS signals.

$$\Delta\rho_I = 40.3\frac{\mathrm{TEC}}{f^2} \quad (1)$$

Previous studies have explored ionospheric corrections designed for single-frequency GNSS receivers, utilizing the thin shell model [32,33]. This model simplifies the three-dimensional ionosphere into a two-dimensional thin shell. The correction accuracy largely relies on the TEC in the ionosphere and generally performs well under quiet space weather. However, during geomagnetic storms, the thin shell model may fail to provide accurate ionospheric corrections, resulting in unacceptably large errors. In this situation, integrity and assured accuracy cannot be guaranteed. Table 1 outlines the requirements of accuracy, integrity, continuity, and availability for aircraft operation at each stage. If any of these requirements are not satisfied, satellite navigation cannot be used.

The Halloween storm in October-November 2003 unleashed a sequence of powerful solar flares and CMEs, resulting in extensive disruptions across numerous technological systems. Within this array of affected domains, GNSS suffered profound consequences, which are crucial for precise positioning and navigation in aviation. An illustrative depiction of the hourly ionospheric TEC map from 27 to 31 October 2003 can be available via https://zenodo.org/records/11112306. Notably, TEC increased significantly within the Continental United States (CONUS) at 20:00 on both October 29 and October 30. Due to data restrictions, we evaluate GNSS performance solely in terms of accuracy rather than integrity, continuity, or availability. Fig. 2 illustrates the positioning errors of nine representative Continuously Operating Reference Stations (CORS) using the solution mode of Single Point Positioning (SPP). For stations such as TMGO, ALBH, MHCB, CNPP, TXAU, and BRTW, two notable spikes in positioning errors coincide with observed increases in TEC on two occasions. Generally, the positioning errors were relatively insignificant in the northeast region of the CONUS, while more pronounced positioning errors were observed elsewhere.

According to [35], the Wide Area Augmentation System (WAAS) was severely affected by the Halloween storm, rendering aircraft unable to utilize WAAS for precise approaches within the CONUS. The primary impact on WAAS was the loss of Localizer Performance with Vertical Guidance (LPV) service, which experienced a suspension period of 15 h, spanning from 17:00 UTC on 29 October 2003–8:00 UTC on 30 October 2003, followed by another interruption lasting approximately 11.3 h, from 19:00 UTC on 30 October 2003–6:20 UTC on 31 October 2003. For example, Fig. 3 shows the non-availability of vertical service in WAAS due to the increased Vertical Protection Level (VPL) on 29 October 2003 [22].

3. Models

This section introduces models related to flight operation in the event of satellite navigation failure. First, the Dijkstra algorithm is introduced for designing a new flight route with the shortest possible flight distance based on ground aids. Subsequently, the fuel consumption model and the aircraft emission model are presented to calculate fuel consumption and aircraft emissions, respectively.

3.1. Flight route design model

In this study, we adopted the Dijkstra algorithm to calculate the shortest paths. Dijkstra provides an exact solution in weighted networks and is commonly used in aviation network analyses as a baseline for route optimization. While more advanced methods, such as A* with heuristic bounding or flow-based and conflict-avoidance path planning, can better capture operational constraints, our focus here is on the theoretical potential of great circle routes. Future work could explore these more realistic routing strategies to assess operational impacts under real-world traffic and conflict scenarios.

To identify realistic aircraft trajectories, a multi-edge directed graph-based airspace network $G(V,E)$ is introduced. Derived from the air navigation dataset, the vertex set V consists of airports, markers, and waypoints, and the edge set E is composed of unidirectional/bidirectional airway segments with various types. Specifically, in response to satellite navigation failures, RNAV airway segments are conditionally incorporated due to their navigation error tolerances during the planning horizon. Additionally, dependencies between nearby vertices are integrated to fulfill operational requirements for specific procedures such as Standard Instrument Departures (SIDs) and Standard Terminal Arrival Routes (STARs), as well as compulsory routes. Moreover, to account for direct flight segments, we include waypoint pairs with distances spanning from 50 km to 80 km. To avoid the surging number of edges, a space-partitioning data structure, i.e. a k-dimensional tree, is introduced for querying neighborhood vertices within the distance threshold. As depicted in Fig. 4, an airspace network comprised of five waypoints (a, b, c, d, and e) and two airports (Origin airport 'O' and Destination airport 'D') possesses multiple kinds of edge types. To reduce computational complexity, only transition fixes (e.g. a, b, and c) associated with certain departure/arrival procedures are considered to facilitate trajectory optimization at the cruising level.

Considering the large size of the complete airspace network, the vertex and edge sets are further confined to focus on the origin and destination airports of a specific flight. To achieve this, $p_1 = (lon_1, lat_1)$ and $p_2 = (lon_2, lat_2)$ are defined as the coordinates of the origin and destination airports, respectively. Then, an ellipse is formulated with p_1 and p_2 be the focus, determining the focal length as $c = \sqrt{(lon_1 - lon_2)^2 + (lat_1 - lat_2)^2}$. By using a varying scaling factor $\theta \in [1.4,\ \ 2.5]$ for the value c, the length of the major axis a is determined as $a = \theta c$, and the length of the minor axis is $b = \sqrt{a^2 - c^2}$. Next, the rotation angle $\phi = \arctan((lat_2 - lat_1)/(lon_2 - lon_1))$ and the ellipse center (lon_0, lat_0) are defined. Subsequently, the boundary of the confined airspace is depicted by points with coordinates of (lon_t, lat_t), $t \in$

Table 1
Signal-in-space performance requirements [34]. APP: Approach; NPA: Non-precision approach; APV: Approach operations with vertical guidance.

Typical operation	Accuracy horizontal 95 %	Accuracy vertical 95 %	Integrity	Time-to-alert	Continuity	Availability
En-route	3.7 km	N/A	$1–1\times10^{-7}$/h	5 min	$1–1\times10^{-4}$/h to $1–1\times10^{-8}$/h	0.99–0.99999
En-route, Terminal	0.74 km	N/A	$1–1\times10^{-7}$/h	15 s	$1–1\times10^{-4}$/h to $1–1\times10^{-8}$/h	0.99–0.99999
Initial APP, Intermediate APP, NPA, Departure	220 m	N/A	$1–1\times10^{-7}$/h	10 s	$1–1\times10^{-4}$/h to $1–1\times10^{-8}$/h	0.99–0.99999
APV-I	16.0 m	20.0 m	$1–2\times10^{-7}$/h	10 s	$1–8\times10^{-6}$ per 15 s	0.99–0.99999
APV-II	16.0 m	8.0 m	$1–2\times10^{-7}$/h	6 s	$1–8\times10^{-6}$ per 15 s	0.99–0.99999
CAT-I precision approach	16.0 m	6.0–4.0 m	$1–2\times10^{-7}$/h	6 s	$1–8\times10^{-6}$ per 15 s	0.99–0.99999

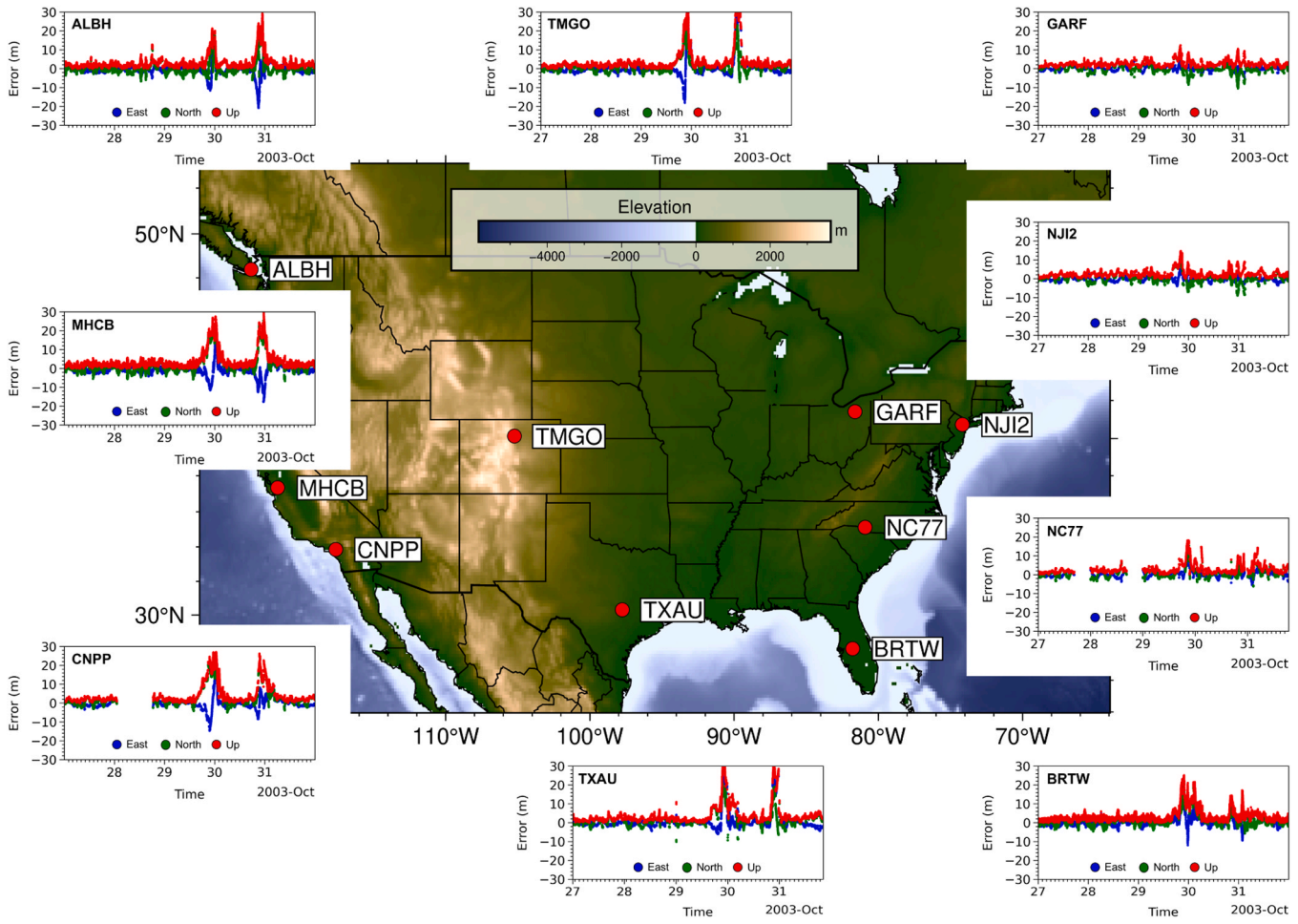

Fig. 2. The positioning errors during 27–31 October 2003 based on the SPP method. The positioning errors for TMGO, ALBH, MHCB, CNPP, TXAU, and BRTW are relatively higher than those for NC77, NJI2, and GARF.

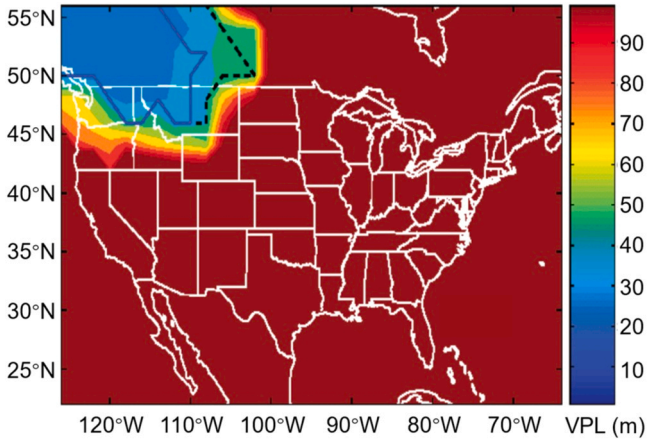

Fig. 3. Vertical service non-availability (VPL is more than 90 m, over the threshold of 50 m) throughout most of the U.S. at 19:06 UTC on 29 October 2003 [22].

$[0,\ 2\pi]$.

$$lon_t = lon_0 + a\cos(t)\cos(\phi) - b\sin(t)\sin(\phi) \tag{2}$$

$$lat_t = lat_0 + a\cos(t)\sin(\phi) + b\sin(t)\cos(\phi) \tag{3}$$

For airports without departure procedures (i.e. those subject to Air

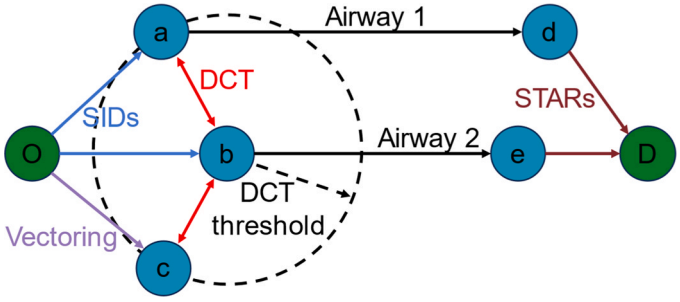

Fig. 4. Illustrative airspace network structure for designing flight routes. DCT denotes direct flights.

Traffic Control (ATC) vectoring), the vertex representing the origin airport of a flight is linked with a maximum of 10 nearby vertices associated with enroute airways to prevent isolation. Based on the airspace network graph, the flight trajectory can be generated by a generic label-setting shortest path algorithm to minimize the traversed distance between two airports. Herein, the distance of each edge is calculated as the great circle distance between the source and target coordinates. The detailed procedure for the adopted algorithm is displayed in **Algorithm 1**. In this context, a heuristic value, denoted as $h(l)$, is assigned to each label, reflecting the direct great circle distance from the current vertex of the label to the destination airport. This heuristic value serves as a lower bound estimation for the actual traversed

distance. To account for potential dependencies between waypoints, a map M is created to prevent deviation from compulsory route segments E_c.

Algorithm 1. : Label setting shortest path algorithm

Input:	Airspace network $G(V,E)$, origin vertex s and destination vertex t
Output:	A flight trajectory with the shortest distance
1	Initialize all labels l_i with cost $c(l_i) \leftarrow \infty$, $i \in V$, $c(l_i) \leftarrow 0$
2	Create priority queue $Q \leftarrow \{l_s\}$ that output label l with decreasing cost $c(l) + h(l)$
3	Create dependency map $M \leftarrow \emptyset$
4	**while** Q is not empty **do**
5	Pop out the top label l_i at vertex i from Q
6	**if** $i = t$ **then**
7	**break**
8	**for** each vertex $(i,j) \in E$ **do**
9	**if** i in M and $M[i] \neq j$ **do**
10	**continue**
11	create new label l_j with cost $c^{temp}(l_j) \leftarrow c(l_j) + c_{ij}$
12	**if** $c(l_j) > c^{temp}(l_j)$ **do**
13	$c^{temp}(l_j) \leftarrow c(l_j)$
14	**if** $(i,j) \in E_c$ **do**
15	$[j] \leftarrow k, (j,k) \in E_c$

The wind speed $\boldsymbol{w}$ plays a crucial role in determining flight time, which in turn affects fuel consumption. The ground speed vector $\boldsymbol{g}$ can be represented as $\boldsymbol{g} = \boldsymbol{w} + \boldsymbol{v}$. As a result, the ground speed (in km/h) can be expressed as $g = |\boldsymbol{w} + \boldsymbol{v}|$. Consequently, the fuel consumption F (in kg) for flying a specific flight distance L (in km) can be calculated by:

3.2. Fuel consumption model

According to BADA [36], the nominal fuel flow f (kg/min) for jet engine aircraft can be determined as a function of thrust-specific fuel consumption η (kg/(min·kN)) and engine thrust Thr (N).

$$f = \frac{\eta \bullet Thr}{1000} \tag{4}$$

where η relies on coefficients C_{f_1} and C_{f_2}, along with the true airspeed (TAS) v (km/h).

$$\eta = C_{f_1}\left(1 + \frac{v}{1.852 \bullet C_{f_2}}\right) \tag{5}$$

During the cruise phase, the drag force D (Newton) is assumed to be equal to the thrust, and the procedure for computing the drag force is delineated in the following formulas.

$$Thr = D \tag{6}$$

$$D = \frac{1}{2} C_D \bullet \rho \bullet \left(\frac{v}{3.6}\right)^2 \bullet S \tag{7}$$

$$C_D = C_{D_0.CR} + C_{D_2.CR} \bullet (C_L)^2 \tag{8}$$

$$C_L = \frac{2 \bullet m \bullet g_0}{\rho \bullet \left(\frac{v}{3.6}\right)^2 \bullet S \bullet \cos\theta} \tag{9}$$

where C_D is the standard drag coefficient, ρ denotes the standard air density (kg/m^3), and S represents the wing reference area (m^2). Moreover, $C_{D_0.CR}$ and $C_{D_2.CR}$ denote specific drag coefficients. The lift coefficient C_L correlates with aircraft mass (m) and bank angle θ.

$$F = 60 \times f \times \frac{L}{g} \tag{10}$$

3.3. Aircraft emission model

The impacts of aircraft emissions on aircraft emissions are extensive and diverse. These emissions consist of various pollutants, such as carbon dioxide (CO_2), water vapor (H_2O), sulfur oxides (SO_x), hydrocarbons (HC), carbon monoxide (CO), nitrogen oxides (NO_x), and particulate matter (PM) [37,38]. These pollutants have significant effects on both local and global environments. Locally, they contribute to the deterioration of air quality and can pose health hazards to communities residing near airports [39-41]. Globally, aircraft emissions play a substantial role in climate change by releasing greenhouse gases into the atmosphere, thereby exacerbating phenomena such as global warming and the depletion of the ozone layer. The emissions can be quantified based on the International Civil Aviation Organization Engine Emissions Databank [42].

$$E_j = F \bullet e_j^f \tag{11}$$

where E_j represents the weight of the specific aircraft emission j measured in kg. The emission indices e_j^f for CO_2, H_2O, and SO_x are standardized at 3.15 kg/kg, 1.25 kg/kg, and 1 g/kg, respectively. However, estimating emissions for other pollutants such as HC, CO, and NO_x is more complex, as these emissions are primarily influenced by combustion parameters and engine power settings [43].

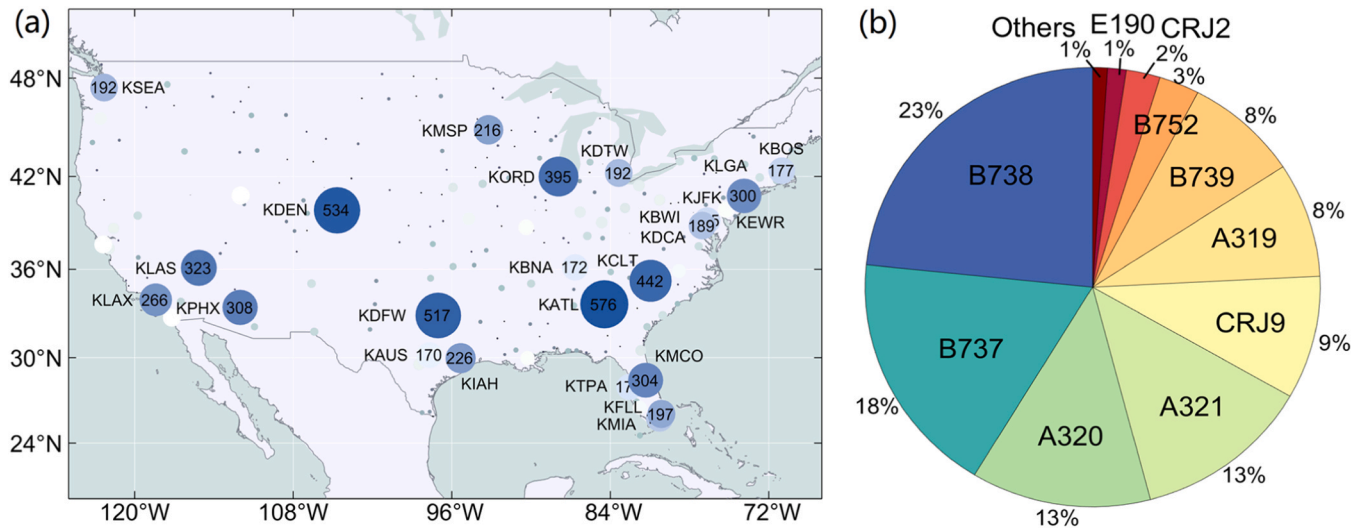

Fig. 5. (a) Aircraft geographical locations denoted by circles and the number of departure flights of each airport, and (b) the percentage of top ten popular aircraft utilization based on the collected flight data.

$$\ln e_j^f = \begin{cases} \dfrac{\left(\ln e_j^{f_{30\%}} - \ln e_j^{f_{7\%}}\right)\left(\ln f - \ln f_{7\%}\right)}{\ln f_{30\%} - \ln f_{7\%}} + \ln e_j^{f_{7\%}}, & f_{7\%} \le f < f_{30\%} \\ \dfrac{\left(\ln e_j^{f_{85\%}} - \ln e_j^{f_{30\%}}\right)\left(\ln f - \ln f_{30\%}\right)}{\ln f_{85\%} - \ln f_{30\%}} + \ln e_j^{f_{30\%}}, & f_{30\%} \le f < f_{85\%} \\ \dfrac{\left(\ln e_j^{f_{100\%}} - \ln e_j^{f_{85\%}}\right)\left(\ln f - \ln f_{85\%}\right)}{\ln f_{100\%} - \ln f_{85\%}} + \ln e_j^{f_{85\%}}, & f_{85\%} \le f \le f_{100\%} \end{cases} \tag{12}$$

4. Datasets

This section lays the foundation for assessing the effects of satellite navigation failure on flight operation by introducing U.S. flight data and wind information. This comprehensive flight data enables detailed analysis of how satellite navigation failure affects various aviation parameters, while wind data provides valuable insights into atmospheric conditions that can influence flight operations and fuel consumption.

4.1. Flight data

This study collects a total of 11,037 flights on 5 February 2024 (UTC), encompassing 3523 unique flight routes connecting 264 airports throughout the United States. Fig. 5(a) visually depicts the spatial distribution of these airports, showcasing the number of departure flights originating from each airport. Fig. 5 depicts the level of air traffic activity of different airports within the U.S. airspace. Specifically, data from 576 departure flights at the Atlanta International Airport (KATL) were obtained on that day, followed by Denver International Airport (KDEN) and Dallas Fort Worth International Airport (KDFW). Fig. 5(b) illustrates the types of aircraft within the collected dataset. B738, B737, A320, and A321 stand out as the most frequently used aircraft types, collectively accounting for 67 %, followed by CRJ9 (9 %), A319 (8 %), and B739 (8 %). By categorizing aircraft based on their respective types and operational characteristics, Fig. 5(b) shows the composition and usage patterns of aviation fleets observed on the specified date, which is important in accurately calculating fuel consumption. It is important to acknowledge that the collected dataset is not complete, and the number of actual flights may be larger than what we have obtained. Despite this limitation, the simulation results derived from the available dataset

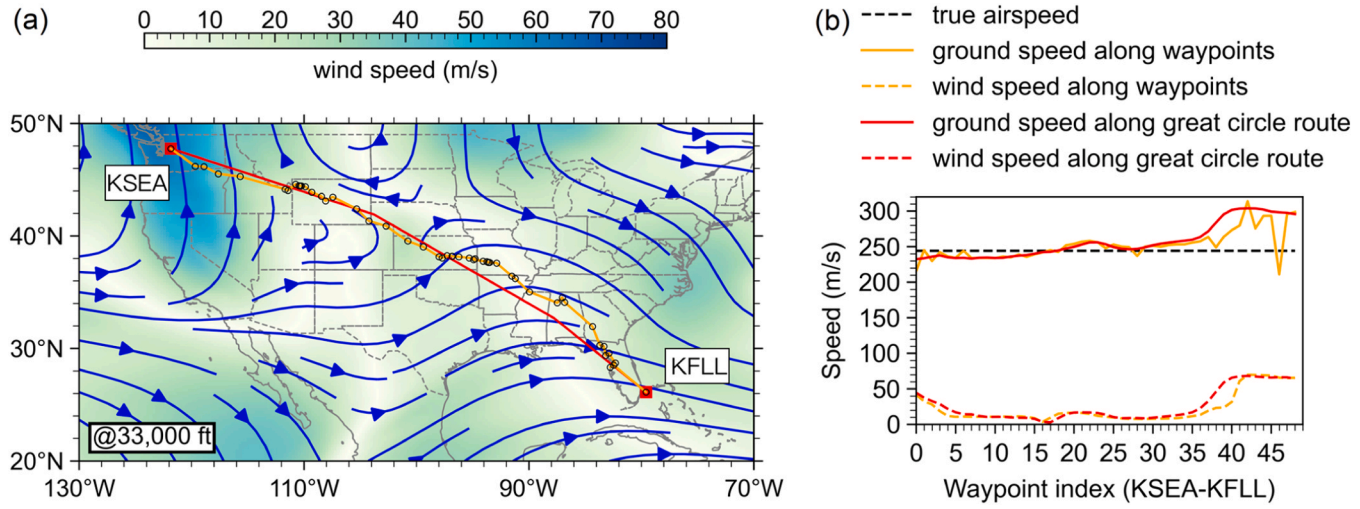

Fig. 6. (a) An example of wind speeds and wind directions in conjunction with the flight route from KSEA to KFLL, with ground aids indicated by circles; (b) ground speeds and wind speeds along the waypoints and great circle routes from KSEA to KFLL.

remain valuable for providing insights into the potential effects of satellite navigation failure. By carefully analyzing the available data and adopting advanced models, we can discern trends and patterns that shed light on the impact of such failures on flight operations.

4.2. Wind data

As mentioned in Section 3.2, wind significantly affects flight time and consequently affects fuel consumption. Herein, wind data is sourced from the European Center for Medium-Range Weather Forecasts (ECMWF) Reanalysis fifth version (ERA5) dataset to provide comprehensive insights into atmospheric conditions. Fig. 6(a) presents a depiction of the spatial distribution of wind at the altitude of 33,000 ft, offering an overview of wind patterns across different geographical regions. Wind directions change significantly in spatial scale. As for the flight from Seattle-Tacoma International Airport (KSEA) to Fort Lauderdale-Hollywood International Airport (KFLL), the aircraft encounters headwinds initially, followed by tailwinds. Fig. 6(b) illustrates the fluctuation of wind speed and ground speed along waypoints and the great circle route, with true airspeed of 245 m/s. A total of 48 ground aids are strategically positioned along the flight route from KSEA to KFLL. Notably, in the final stages of flight, ground speeds along waypoints undergo significant variations, which can be explained by the pronounced change in flight direction.

5. Simulation analysis

This section discusses the effects of satellite navigation failure on fuel consumption and aircraft emissions, through the scenario simulation. Subsequently, a comparative analysis of economic losses across different air traffic management strategies is conducted.

5.1. Scenario simulation

The effects of space weather events can vary in duration, lasting from mere seconds to several days. To mitigate the impacts of space weather on aviation, the space weather advisory services are offered by four global space weather centers. These include the Pan-European Consortium for Aviation Space Weather User Services (PECASUS) formed by Finland, Belgium, the United Kingdom, Austria, Germany, Italy, the Netherlands, Poland, Cyprus, and South Africa; the NOAA Space Weather Prediction Center (SWPC); the consortium formed by Australia, Canada, France, and Japan (ACFJ); and the consortium formed by China and Russia (CRC). These centers operate on a rotational basis, with one serving as the on-duty center and the others as the primary and secondary backup centers and the maintenance center, each monitoring space weather conditions in a two-week shift.

Table 2
An example of a space weather advisory for GNSS. This advisory was issued by ACFJ at 23:21 (UT) on 25 October 2022, which indicates that space weather (scintillation) is in progress, possibly impacting GNSS performance.

DTG:	20221025/2321Z
SWXC:	ACFJ
ADVISORY NR:	2022/31
SWX EFFECT:	GNSS MOD
OBS SWX:	25/2245Z EQN EQS W090-E015
FCST SWX + 6 HR:	26/0500 NOT AVBL
FCST SWX + 12 HR:	26/1100 NOT AVBL
FCST SWX + 18 HR:	26/1700 NOT AVBL
FCST SWX + 24 HR:	26/2300 NOT AVBL
RMK:	SWX ENENT (SCINTILATION) INPR POSSIBLY IMPACTING GNSS PER.
NXT ADVISORY	Will be issued by 20221026/0521Z=

Currently, the space weather advisory service focuses on three main areas related to aviation: HF Communications (HF COM), GNSS-based navigation and surveillance (GNSS), and radiation impacts on avionics and human health (RADIATION). A fourth impact area (SATCOM) has been identified, but advisories for SATCOM so far have not been issued by any space weather centers until further research is conducted to develop and validate operationally relevant advisory thresholds for this impact area. Advisories are issued at either of two intensity thresholds: Moderate (MOD) and Severe (SEV), with alerting thresholds defined in the ICAO Manual on Space Weather Information in Support of International Air Navigation (ICAO Doc 10100) [44]. For instance, Table 2 provides the space weather advisory concerning the impact of space weather on GNSS. This advisory is a warning that a space weather event involving scintillation is currently in progress, and it might be causing interference or degradation in GNSS signal performance. This can affect applications that rely on satellite navigation, such as aviation, maritime, and personal GPS devices. The forecast indicates that GNSS-based operations within the equatorial latitudes of the northern hemisphere (EQN) and southern hemisphere (EQS), spanning from W015° to E015°, will be unavailable for the following 6, 12, 18, and 24 h.

Within this study, we conduct simulations of satellite navigation failure scenarios to investigate their effects on flight operation. In reality, the duration of satellite navigation failures cannot be precisely predicted, as it depends on the intensity of solar activity. Therefore, the scenarios were defined with varying durations: Scenario 1 (S1) from 19:00–21:00 (UT), Scenario 2 (S2) from 16:00–23:59 (UT), and Scenario 3 (S3) from 00:00–23:59 (UT). Through the exploration of these scenarios, our goal is to understand the impact of satellite navigation failure and compare the economic losses incurred with different air traffic management strategies. By simulating various scenarios and analyzing the corresponding results, we seek to provide valuable insights to mitigate the consequences of satellite navigation failure and enhance the sustainability of aviation operations.

5.2. Fuel consumption and aircraft emissions

In response to satellite navigation failure, a newly designed flight route based on ground aids is necessary. Fig. 7 offers a comprehensive view of the challenges inherent in trajectory optimization by depicting airspace networks for two typical points, each traversed in both directions. As flight distances increase, optimizing long-haul routes (KLAX↔KJFK) presents a vastly expanded solution space compared to short-haul flights (KATL↔KFLL). This complexity cannot be simply alleviated by focusing solely on vertices along the great circle curve between origin and destination, where detours may be necessitated by spatial and temporal constraints. Furthermore, variations in trajectory patterns for symmetric origin-destination pairs underscore the nuanced influence of SIDs, STARs, and airways on route configuration, particularly when transition points and operational directions differ. Another pertinent consideration lies in the distance differences between designed flight routes, exemplified by KATL→KFLL (1200 km) and KFLL→KATL (1273 km), with the satellite navigation-based great circle route distance for the cruising phase between KATL and KFLL standing at 935 km. Similarly, Fig. 7(c) and (d) show the designed flight routes of KLAX→KJFK (4120 km) and KJFK→KLAX (4053 km), with the satellite navigation-based great circle route distance of 3983 km. Using the flight data during the whole day, Fig. 8 shows the hourly results of flight distance, fuel consumption, and different aircraft emissions based on ground navigation and satellite navigation. Overall, all parameters have increased by an average of 15 %, as the flight distance has increased by an average of 15 %, indicating the effects of satellite navigation failure on flight operation.

To quantify the effects of different scenarios of satellite navigation failure, Table 3 presents a comprehensive analysis of flight distance, fuel consumption, flight time, and emissions based on satellite navigation and ground navigation. Specifically, in Scenario 3 (S3), the total flight

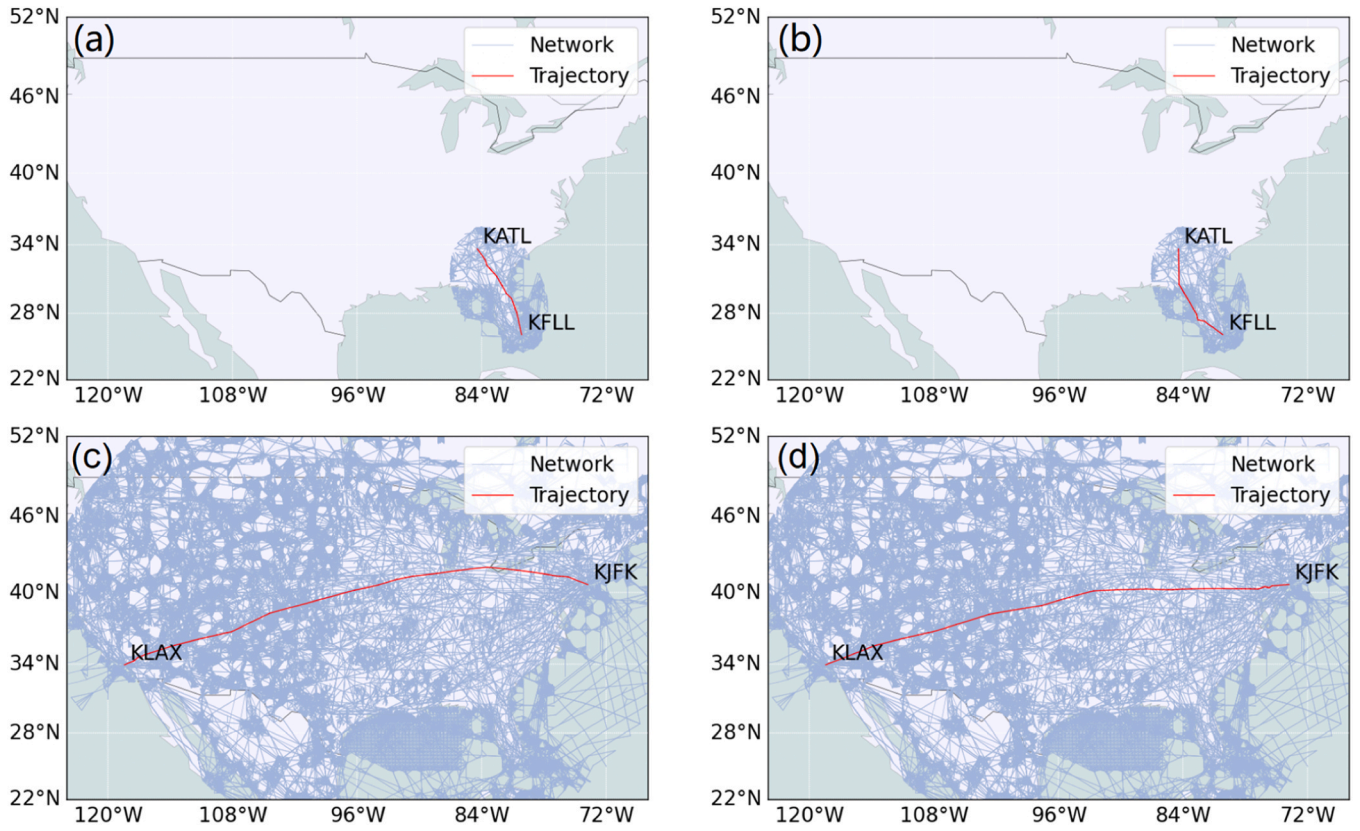

Fig. 7. Designed flight route based on ground aids for (a) KATL→KFLL (1200 km), (b) KFLL→KATL (1273 km), (c) KLAX→KJFK (4120 km), and (d) KJFK→KLAX (4053 km).

distance exhibits a substantial increase of 2,371,777 km, accompanied by an additional fuel consumption of 7176 tons and flight time of 174,653 min. This shows that with the prolonged duration of satellite navigation failure, all analyzed parameters consistently demonstrate an increase.

5.3. Airline economic loss

This section aims to evaluate the comprehensive economic impacts on airlines by examining various ATM strategies. These strategies include flight cancellation, rescheduling, and rerouting. By analyzing these approaches, our objective is to assess the potential economic losses across different scenarios (S1, S2, and S3).

5.3.1. Flight cancellation loss

Flight cancellations stemming from satellite navigation failure caused by space weather present a significant challenge to both airlines and the broader economy. When space weather events disrupt satellite-based navigation systems, airlines may be forced to cancel flights to uphold safety standards. This abrupt disruption in flight schedules can lead to substantial economic losses for airlines, encompassing not only the immediate costs associated with ticket refunds but also the long-term impact on revenue streams. Moreover, the ripple effects of flight cancellations extend beyond airlines to impact various sectors of the economy reliant on air transportation, including tourism, business travel, and supply chain logistics. It is important to emphasize that space weather events are beyond human control, and according to [45], airlines are not obligated to compensate passengers for disruptions caused by these events. However, other associated costs cannot be avoided, including loss of revenue, interlining costs, loss of future value, crew and catering expenses, luggage delivery fees, etc. Table 4 provides the seat capacities and cancellation costs [46] for each aircraft type, along with the number of affected flights in various scenarios. Consequently, the economic loss incurred by airlines due to flight cancellations in simulation scenarios S1, S2, and S3 amount to €27.21 million, €67.75 million, and €114.62 million, respectively. It should be noted that this estimation is based on the 11,037 flights for which we have obtained data. The actual number of flights is larger than 11,037 and the economic losses should be larger too.

5.3.2. Flight rescheduling loss

Another ATM strategy in response to satellite navigation failure is flight rescheduling, aimed at adjusting the flight departure time to avoid encountering satellite navigation failure during the flight. In scenario i, the start and ending times of satellite navigation failure are denoted by S_i, and E_i, respectively. For flight j, the original departure and landing times are represented by d_j and l_j, respectively. Due to satellite navigation failure, the rescheduled departure and landing times are denoted by $d_j^{'}$ and $l_j^{'}$, respectively. The flight does not depart until the satellite navigation failure ends, i.e. $d_j^{'} = E_i$. In scenario i, the ground delay time for flight j (in the units of minutes) is calculated as $P_j = d_j^{'} - d_j = E_i - d_j$. Given the ground delay cost of airlines at €16 per minute [46], the economic loss on airlines resulting from rescheduling flight j is $D_j = 16P_j$, where P_j is 331,119 min (S1), 1,938,640 min (S2), and 6,711,390 min (S3), and subsequently the total the economic loss on airlines in simulation scenarios S1, S2, and S3 is calculated at €5.30 million, €31.02 million, and €170.38 million, respectively. Again, it should be noted that this estimation is based on the data of 11,037 flights. The actual number of flights is larger than 11,037 and the economic losses should be larger, too.

5.3.3. Flight rerouting loss

In the event of satellite navigation failure, aircraft may opt to reroute using ground aids, as outlined in Section 5.2. The economic effects of flight rerouting on airlines are considered in terms of additional fuel

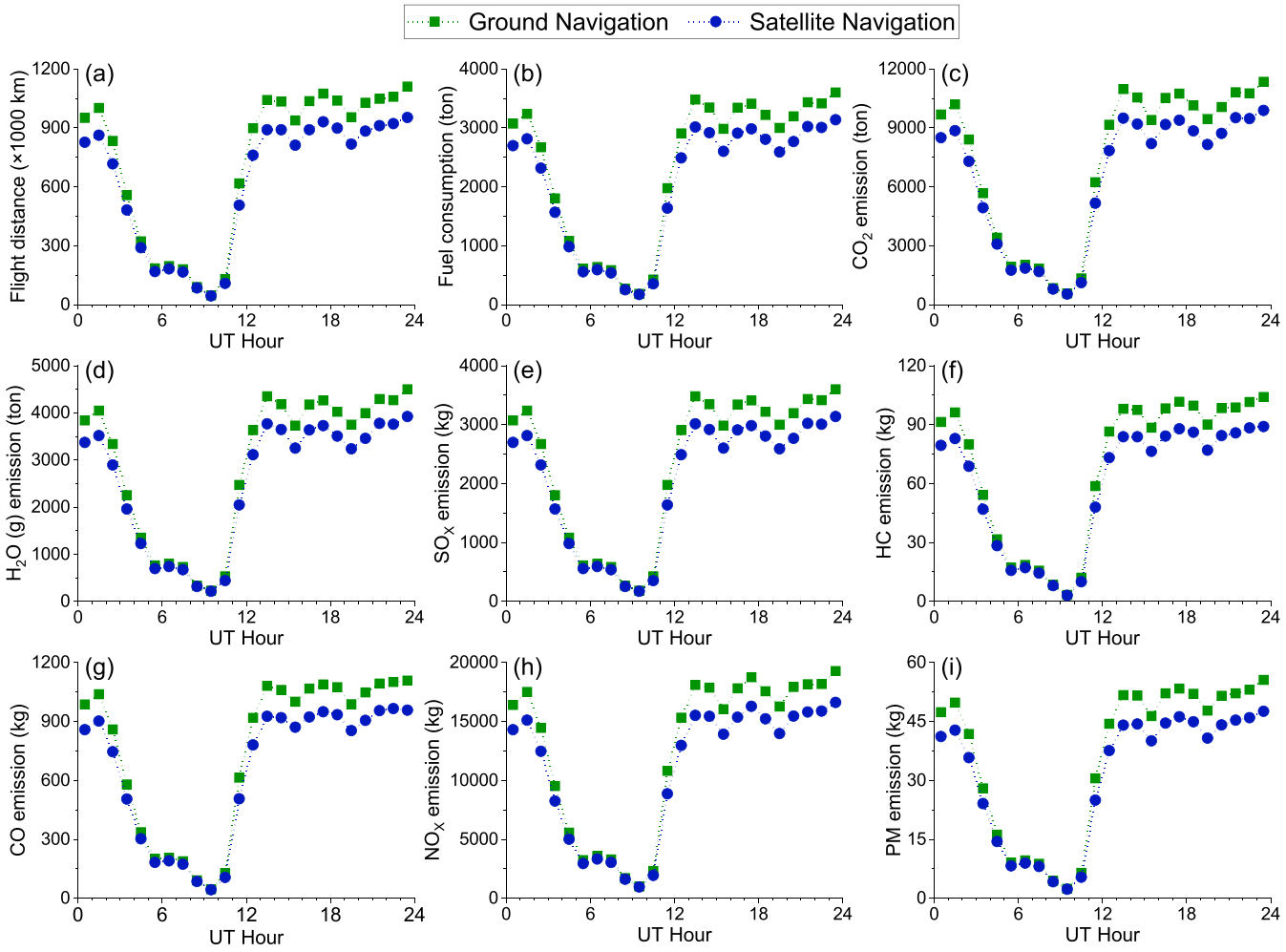

Fig. 8. Hourly results of flight distance (a), flight fuel (b), and various aircraft emissions (c)-(i) based on ground navigation and satellite navigation.

Table 3
Results of total flight distance, flight fuel, and emissions based on satellite navigation and ground navigation in different satellite navigation failure scenarios.

	S1		S2		S3	
Parameter	Sat. Nav.	Gnd. Nav.	Sat. Nav.	Gnd. Nav.	Sat. Nav.	Gnd. Nav.
Flight distance (km)	1,700,011	1,981,160	7,201,479	8,342,829	14,984,541	17,356,318
Fuel consumption (ton)	5353	6191	23,209	26,607	48,677	55,853
Flight time (min)	304,284	347,175	715,687	820,356	1,142,452	1,317,105
CO_2 (ton)	16,862	19,502	73,108	83,812	153,333	175,937
H_2O (g) (ton)	6691	7739	29,011	33,259	60,846	69,816
SO_X (kg)	5353	6191	23,209	26,607	48,677	55,853
HC (kg)	161	188	682	792	1422	1649
CO (kg)	1758	2034	7438	8564	15,527	17,885
NO_X (kg)	29,411	34,175	124,552	143,838	260,031	300,336
PM (kg)	85	99	359	417	745	865

costs and increased flight time. Fuel expenses represent a significant expense for airlines, given a fuel price of €843 per ton [47], while flight time costs, valued at €74 per minute [46], also contribute to the economic loss for airlines. For flight j, the total economic loss can be represented as $R_j = 843\Delta F_j + 74\Delta T_j$, where ΔF_j denotes the increased fuel consumption, ΔT_j represents the increased flight time. Based on the fuel consumption and flight time listed in Table 3, the economic loss incurred by airlines due to flight rerouting in S1, S2, and S3 amounts to €4.70 million, €11.36 million, and €18.97 million, respectively. The actual number of flights is larger than 11,037. Thus the actual economic losses will be larger than these numbers.

5.3.4. Minimum economic loss

When examining the economic losses associated with the three ATM strategies, it is clear that rerouting flights tends to result in the least economic loss, whereas flight cancellations lead to the most significant economic losses. Nonetheless, the optimal choice between these strategies may vary depending on the specific characteristics of a given flight j. To address this variability, we introduce the concept of minimum economic loss for each flight, denoted as $M_j = \min\{C_j, D_j, R_j\}$, where C_j, D_j, and R_j represent the economic losses associated with airlines due to flight cancellation, delay (rescheduling), and rerouting, respectively. It should be noted that for each flight, the best ATM strategy to minimize

Table 4
The seat capacities and cancellation costs [46] of each aircraft type and the number of affected flights in different scenarios. The cancellation loss for aircraft j is denoted by C_j.

Aircraft type	Seat capacity	Cancellation loss per aircraft (€) C_j	Number of canceled flights		
			S1	S2	S3
A319	128	8525	216	547	930
A320	150	9915	338	806	1410
A321	182	12,615	334	803	1394
A332	332	46,796	1	2	4
A333	293	43,559	1	3	4
B737	143	9473	431	1176	1980
B738	181	12,213	599	1492	2580
B739	167	10,989	229	533	896
B752	169	11,115	80	189	316
B763	214	25,497	11	22	29
B772	336	47,128	18	43	56
B788	234	33,549	5	10	12
B789	252	40,156	4	8	11
CRJ2	52	3396	54	167	266
CRJ9	76	5028	211	599	1002
E190	100	6660	31	90	147

Table 5
The economic losses of airlines and passengers, and CO_2 social cost due to flight cancellation, rescheduling (delay), and rerouting in different scenarios (million Euros).

Scenarios	Strategies	Airlines	Passengers	CO_2	Total
S1	Cancellation	27.21	X_1	−7.70	19.51 +X_1
	Rescheduling	5.30	77.27	0	82.57
	Rerouting	4.70	4.13	4.56	13.39
S2	Cancellation	67.75	X_2	−17.86	49.89 +X_2
	Rescheduling	31.02	185.92	0	216.94
	Rerouting	11.36	9.93	11.02	32.31
S3	Cancellation	114.62	X_3	−28.37	86.25 +X_3
	Rescheduling	170.38	642.18	0	812.56
	Rerouting	18.97	16.57	18.42	53.96

the economic loss might be different, depending on the original flight distance, aircraft type, original flight schedule, the duration of satellite navigation failure, the extent of increased flight distance resulting from rerouting, and others.

Our investigation reveals that the overall minimum economic losses for all the 11,037 flights amount to €2.92 million, €9.44 million, and €17.04 million in the simulation scenarios S1, S2, and S3, respectively. This is a significant reduction compared to adopting one single uniform ATM strategy for all the flights in each scenario. This shows the importance of airlines making informed decisions tailored to the specific circumstances of satellite navigation failure. Factors such as aircraft types, the extent of increased flight distance resulting from rerouting, original flight schedules, and the duration of satellite navigation failure must all be carefully weighed in selecting the most suitable course of action. By prioritizing such considerations, airlines can mitigate economic losses and ensure the efficient management of disruptions caused by satellite navigation failure.

5.4. Total economic loss

In addition to the economic losses incurred by airlines, flight rescheduling (delays) and rerouting can also result in time costs for passengers. Moreover, flight rerouting may contribute to increased social costs associated with CO_2 emissions. Therefore, Table 5 provides a summary of the economic losses of airlines and passengers, as well as CO_2 social costs due to flight cancellation, rescheduling (delay), and rerouting in different scenarios. It is important to highlight that the economic losses incurred by airlines were discussed in Section 5.3. Using an average passenger time value of €47 per hour [48] and considering an 80 % seat occupancy factor, the time costs arising from flight rescheduling and rerouting can be computed. However, accurately quantifying the economic losses experienced by passengers due to flight cancellations proves challenging. Therefore, we adopt X_1, X_2, and X_3 to denote the economic losses of passengers in scenarios S1, S2, and S3, respectively. It should be noted that this study does not provide estimates of passenger cancellation costs, as the necessary statistical data from airlines is not publicly available. Another significant aspect is the social cost of CO_2 emissions, estimated at $185 per ton [49]. It is noteworthy that flight rescheduling does not contribute to additional fuel consumption, resulting in zero economic loss related to CO_2 social costs. Compared to rerouting, cancellation can lead to a reduction in CO_2 emissions, resulting in savings of CO_2 social costs amounting to €7.70 million, €17.86 million, and €28.37 million in scenarios S1, S2, and S3, respectively.

6. Discussions and implications

This study shows that satellite navigation failures caused by space weather can significantly affect aviation operations. Even short-term outages can increase flight distances, fuel use, and emissions, while longer disruptions amplify both operational inefficiencies and economic costs. These findings highlight the vulnerability of aviation systems to solar activity and underscore the importance of preparing for the upcoming solar maximum in 2025. The comparative evaluation of ATM strategies indicates that economic outcomes vary with the chosen response. Flight cancellations tend to cause the highest losses, while rerouting generally produces the lowest. Rescheduling can be effective in some cases but may generate substantial ground delay costs. These results suggest that flexible, context-specific decision-making is essential, as the effectiveness of each strategy depends on outage duration, flight schedules, aircraft types, and rerouting distances.

In addition to satellite navigation failures, Xue [50] has concluded that space weather can also disrupt aviation through high-frequency communication blackouts [51-53], surveillance system anomalies [54, 55], and more aviation radiation exposure [56-58]. Given the considerable economic risks of the solar maximum, several operational recommendations can be made for industry stakeholders. First, enhancing space weather monitoring and forecasting capabilities will enable proactive responses to disruptions. Second, airlines should integrate contingency planning, such as flexible rescheduling and rerouting protocols, into routine operations. Third, strengthening ground-based navigation infrastructure can provide resilience when satellite navigation is degraded. Finally, international coordination between space weather agencies, regulators, and service providers is crucial to harmonize responses and disseminate best practices. By combining quantitative evidence with practical recommendations, this study provides actionable insights to support airlines, regulators, and service providers in mitigating risks, reducing economic losses, and enhancing aviation resilience during space weather events. For detailed information related to space weather impacts on other transportation systems, please refer to [59].

7. Conclusions

This study evaluated the impacts of space weather-induced satellite navigation failures on aviation operations, focusing on fuel consumption, emissions, and economic losses. Using more than 11,000 U.S. flight plans, the simulations show that even short-term outages can lead to significant increases in flight distances and operational costs, while prolonged disruptions may amplify these effects to a scale that challenges aviation resilience. The analysis of alternative ATM strategies highlights the importance of adaptive decision-making. While rerouting generally minimized losses, rescheduling and cancellations introduced considerable economic trade-offs. These results underscore that the

effectiveness of any strategy depends on outage duration, aircraft type, and traffic demand.

The findings provide quantitative evidence of aviation's vulnerability to space weather and carry important implications for industry stakeholders as the solar maximum approaches. Strengthening forecasting systems, embedding contingency planning into airline operations, maintaining ground-based navigation capabilities, and fostering international coordination are essential to mitigate operational and economic risks. By linking scientific assessment with practical recommendations, this study contributes to both advancing academic understanding and guiding industry preparedness for sustainable and resilient aviation under space weather challenges.

CRediT authorship contribution statement

Yifan Xu: Writing – original draft, Visualization, Validation, Formal analysis, Data curation. **Dabin Xue:** Writing – original draft, Methodology, Formal analysis, Data curation, Conceptualization. **Zhizhao Liu:** Writing – review & editing, Visualization, Validation, Formal analysis, Data curation. **Shiwei Yu:** Writing – original draft, Visualization, Methodology, Formal analysis, Data curation.

Declaration of Competing Interest

The authors declare that they have no known competing financial interests or personal relationships that could have appeared to influence the work reported in this paper.

Acknowledgements

This work was partially supported by the State Key Laboratory of Climate Resilience for Coastal Cities at the Hong Kong Polytechnic University. The Research Grants Council of Hong Kong Special Administrative Region, China (under Project PolyU/RGC 15212622/B-Q94L) and the Hong Kong Polytechnic University (under Project 4-ZZVL) are acknowledged for partially supporting this work. This work was also partially supported by the Otto Poon Research Institute for Climate-Resilient Infrastructure (RICRI) at the Hong Kong Polytechnic University (project ZH8Y).

Data availability

Data will be made available on request.

References

[1] K. Samalla, P.N. Kumar, Global navigation satellite system in the civil surveillance, ACS J. Sci. Eng. 4 (1) (2024) 1–10.
[2] D. Xue, L.-T. Hsu, C.-L. Wu, C.-H. Lee, K.K. Ng, Cooperative surveillance systems and digital-technology enabler for a real-time standard terminal arrival schedule displacement, Adv. Eng. Inform. 50 (2021) 101402.
[3] P. Enge, N. Enge, T. Walter, L. Eldredge, Aviation benefits from satellite navigation, N. Space 3 (1) (2015) 19–35.
[4] V. Demyanov, Y.V. Yasyukevich, Space weather: risk factors for global navigation satellite systems, Sol. Terr. Phys. 7 (2) (2021) 28–47.
[5] B. Roy, A. Paul, Impact of space weather events on satellite-based navigation, Space Weather 11 (12) (2013) 680–686.
[6] J. Eastwood, E. Biffis, M. Hapgood, L. Green, M. Bisi, R. Bentley, R. Wicks, L. A. McKinnell, M. Gibbs, C. Burnett, The economic impact of space weather: where do we stand? Risk Anal. 37 (2) (2017) 206–218.
[7] D.C. Ferguson, S.P. Worden, D.E. Hastings, The space weather threat to situational awareness, communications, and positioning systems, IEEE Trans. Plasma Sci. 43 (9) (2015) 3086–3098.
[8] A. Papaioannou, I. Sandberg, A. Anastasiadis, A. Kouloumvakos, M.K. Georgoulis, K. Tziotziou, G. Tsiropoula, P. Jiggens, A. Hilgers, Solar flares, coronal mass ejections and solar energetic particle event characteristics, J. Space Weather Space Clim. 6 (2016) A42.
[9] V. Sreeja, Impact and mitigation of space weather effects on GNSS receiver performance, Geosci. Lett. 3 (1) (2016) 24.
[10] A.J. Coster, E. Yizengaw, GNSS/GPS degradation from space weather, Space Weather Eff. Appl. (2021) 165–181.
[11] A. Singh, D. Siingh, R. Singh, Space weather: physics, effects and predictability, Surv. Geophys. 31 (2010) 581–638.
[12] A.K. Singh, A. Bhargawa, D. Siingh, R.P. Singh, Physics of space weather phenomena: a review, Geosciences 11 (7) (2021) 286.
[14] X. Wang, L. Dai, T. Wang, Y. Ren, M. Zhu, X. Yang, C. Wang, W. Gonzalez, Inner magnetospheric convection electric fields and corresponding geomagnetic indices during high-speed solar wind streams, Space Weather 23 (8) (2025) e2025SW004548.
[13] L. Dai, M. Zhu, Y. Ren, W. Gonzalez, C. Wang, D. Sibeck, A. Samsonov, P. Escoubet, B. Tang, J. Zhang, Global-scale magnetosphere convection driven by dayside magnetic reconnection, Nat. Commun. 15 (1) (2024) 639.
[15] F. Huang, J. Lei, X. Yue, Z. Li, N. Zhang, Y. Cai, S.R. Zhang, Y. Wang, J. Zhong, X. Luan, Interplay of gravity waves and disturbance electric fields to the abnormal ionospheric variations during the 11 May 2024 superstorm, AGU Adv. 6 (1) (2025) e2024AV001379.
[16] Y. Wang, H. Le, L. Liu, Y. Chen, B. Xiong, R. Zhang, B. Liu, W. Li, W. Sun, Y. Li, Mapping the ionosphere over east Asia based on ground-based GNSS TEC data in 2010–2023, Space Weather 23 (7) (2025) e2025SW004343.
[17] E. Blanch, S. Marsal, A. Segarra, J. Torta, D. Altadill, J. Curto, Space weather effects on earth's environment associated to the 24–25 October 2011 geomagnetic storm, Space Weather 11 (4) (2013) 153–168.
[18] A. Danilov, Ionospheric F-region response to geomagnetic disturbances, Adv. Space Res. 52 (3) (2013) 343–366.
[19] Y. Zou, Ionospheric scintillations at guilin detected by GPS ground-based and radio occultation observations, Adv. Space Res. 47 (6) (2011) 945–965.
[20] P. Amaechi, E. Oyeyemi, A. Akala, Geomagnetic storm effects on the occurrences of ionospheric irregularities over the African equatorial/low-latitude region, Adv. Space Res. 61 (8) (2018) 2074–2090.
[21] D. Chen, W. Guo, Z. Xie, P. Xia, X. Luo, S. Ye, W. Jiang, H. Liu, Ionospheric irregularities responses to strong geomagnetic storms in Hong Kong region over the past two solar cycles (2001–2020), IEEE Trans. Geosci. Remote Sens. 61 (2023) 1–9.
[22] National Research Council, Severe Space Weather Events: Understanding Societal and Economic Impacts: A Workshop Report, The National Academies Press, *Washington, DC*, 2008. ⟨https://ui.adsabs.harvard.edu/link_gateway/2008sswe.rept....N/doi:10.17226/12507⟩.
[23] A.D. Hands, K.A. Ryden, N.P. Meredith, S.A. Glauert, R.B. Horne, Radiation effects on satellites during extreme space weather events, Space Weather 16 (9) (2018) 1216–1226.
[24] A. Coster, A. Komjathy, Space weather and the global positioning system, Space Weather 6 (6) (2008).
[25] B.T. Tsurutani, G.P. Zank, V.J. Sterken, K. Shibata, T. Nagai, A.J. Mannucci, D. M. Malaspina, G.S. Lakhina, S.G. Kanekal, K. Hosokawa, Space plasma physics: a review, IEEE Trans. Plasma Sci. 51 (7) (2022) 1595–1655.
[26] Z. Jakšić, M. Janić, Modeling resilience of the ATC (Air Traffic Control) sectors, J. air Transp. Manag. 89 (2020) 101891.
[27] D. Xue, J. Yang, Z. Liu, Potential impact of GNSS positioning errors on the Satellite-Navigation-Based air traffic management, Space Weather 20 (7) (2022) e2022SW003144.
[28] D. Xue, J. Yang, Z. Liu, S. Yu, Examining the economic costs of the 2003 halloween storm effects on the north hemisphere aviation using flight data in 2019, Space Weather 21 (3) (2023) e2022SW003381.
[29] D. Xue, J. Yang, Z. Liu, W. Cong, Forward-Looking study of solar maximum impact in 2025: effects of satellite navigation failure on aviation network operation in the greater bay area, China, Space Weather 21 (12) (2023) e2023SW003678.
[30] J.G. Luhmann, Y. Li, C.O. Lee, L. Jian, C.N. Arge, P. Riley, Solar cycle variability in coronal holes and their effects on solar wind sources, Space Weather 20 (10) (2022) e2022SW003110.
[31] B. Swiger, M. Liemohn, N. Ganushkina, S. Dubyagin, Energetic electron flux predictions in the Near-Earth plasma sheet from solar wind driving, Space Weather 20 (11) (2022) e2022SW003150.
[32] W. Fu, T. Yokoyama, N. Ssessanga, G. Ma, M. Yamamoto, Nighttime midlatitude E-F coupling in geomagnetic conjugate ionospheres: a double thin shell model and a Multi-Source data investigation, J. Geophys. Res. Space Phys. 128 (3) (2023) e2022JA031074.
[33] Z. Huang, H. Yuan, Analysis and improvement of ionospheric thin shell model used in SBAS for China region, Adv. Space Res. 51 (11) (2013) 2035–2042.
[34] ICAO, 2018a. ICAO Annex 10 Volume 1 Radio Navigation Aids. International Civil Aviation Organization. ⟨https://ffac.ch/wp-content/uploads/2020/09/ICAO-Annex-10-Aeronautical-Telecommunications-Vol-I-Radio-Navigation-Aids.pdf⟩.
[35] P. Doherty, A.J. Coster, W. Murtagh, Space weather effects of October-November 2003, GPS Solut. 8 (4) (2004) 267–271.
[36] Eurocontrol, 2022. User manual for the Base of Aircraft Data (BADA) revision 3.16. ⟨https://www.eurocontrol.int/model/bada⟩.
[37] C. Wey, C.-M. Lee, Aircraft emissions: gaseous and particulate, Green Aviat. Reduct. Environ. Impact Aircr. Technol. Altern. fuels 48 (2017). ⟨https://www.taylorfrancis.com/chapters/edit/10.1201/b20287-3/aircraft-emissions-gaseous-particulate-changlie-wey-chi-ming-lee⟩.
[38] D. Xue, Z. Liu, B. Wang, J. Yang, Impacts of COVID-19 on aircraft usage and fuel consumption: a case study on four Chinese international airports, J. Air Transp. Manag. 95 (2021) 102106.
[39] L. Fajersztajn, M.T. Guimaraes, E. Duim, T.G.V. da Silva, M.N. Okamura, S.L. B. Brandão, A.E. Ribeiro, L.M. Naud, S. O'sullivan, P.H.N. Saldiva, Health effects of pollution on the residential population near a Brazilian airport: a perspective based on literature review, J. Transp. Health 14 (2019) 100565.

[40] M. Masiol, R.M. Harrison, Aircraft engine exhaust emissions and other airport-related contributions to ambient air pollution: a review, Atmos. Environ. 95 (2014) 409–455.
[41] S.H. Yim, M.E. Stettler, S.R. Barrett, Air quality and public health impacts of UK airports. Part II: impacts and policy assessment, Atmos. Environ. 67 (2013) 184–192.
[42] ICAO, 2023. Aircraft Engine Emissions Databank. ⟨https://www.easa.europa.eu/en/domains/environment/icao-aircraft-engine-emissions-databank⟩.
[43] ICAO, 2020. DOC 9889, Airport Air Quality Manual, Second Edition. ⟨https://standart.aero/en/icao/book/doc-9889-airport-air-quality-manual-en-cons⟩.
[44] ICAO, 2018b. Manual on space weather information in support of international air navigation. ⟨https://www.icao.int/airnavigation/METP/Panel%20Documents/Doc.10100.Space%20Weather%20Manual%20FINAL%20DRAFT%20Version.pdf⟩.
[45] U.S. Department of Transportation, 2022. Flight Delays & Cancellations. ⟨https://www.transportation.gov/individuals/aviation-consumer-protection/flight-delays-cancellations#:~:text=Some%20problems%2C%20like%20bad%20weather,flights%20are%20delayed%20or%20cancelled⟩.
[46] Eurocontrol, 2020. Standard Inputs for Economic Analyses. ⟨https://www.eurocontrol.int/publication/eurocontrol-standard-inputs-economic-analyses⟩.
[47] IATA, 2024. Jet Fuel Price Monitor. ⟨https://www.iata.org/en/publications/economics/fuel-monitor/⟩.
[48] Airlines for America, 2023. U.S. passenger carrier delay costs. ⟨https://www.airlines.org/dataset/u-s-passenger-carrier-delay-costs/#:~:text=In%202022%2C%20the%20average%20cost,percent%20to%20%2442.15%20per%20min⟩.
[49] K. Rennert, F. Errickson, B.C. Prest, L. Rennels, R.G. Newell, W. Pizer, C. Kingdon, J. Wingenroth, R. Cooke, B. Parthum, Comprehensive evidence implies a higher social cost of CO2, Nature 610 (7933) (2022) 687–692.
[50] D. Xue, Space weather disrupts aviation, npj Space Explor. 1 (1) (2025) 7.
[51] R.A. Fiori, V.V. Kumar, D.H. Boteler, M.B. Terkildsen, Occurrence rate and duration of space weather impacts on high-frequency radio communication used by aviation, J. Space Weather Space Clim. 12 (2022) 21.
[52] N.A. Frissell, J.S. Vega, E. Markowitz, A.J. Gerrard, W.D. Engelke, P.J. Erickson, E. S. Miller, R.C. Luetzelschwab, J. Bortnik, High-frequency communications response to solar activity in September 2017 as observed by amateur radio networks, Space Weather 17 (1) (2019) 118–132.
[53] D. Xue, Z. Liu, D. Zhang, C.-L. Wu, J. Yang, Optimizing polar air traffic: strategies for mitigating the effects of space weather-induced communication failures poleward of 82°N, Space Weather 22 (2024) e2024SW004136.
[54] C. Marqué, K.-L. Klein, C. Monstein, H. Opgenoorth, A. Pulkkinen, S. Buchert, S. Krucker, R. Van Hoof, P. Thulesen, Solar radio emission as a disturbance of aeronautical radionavigation, J. Space Weather Space Clim. 8 (2018) A42.
[55] E. Schmölter, J. Berdermann, V. Wilken, D. Wenzel, Should we monitor space weather effects on surveillance technologies used in air traffic management?—First results, Space Weather 23 (4) (2025) e2025SW004352.
[56] H. Bain, T. Onsager, C. Mertens, K. Copeland, E. Benton, J. Clem, P.-S. Mangeard, J. Green, T. Guild, W. Tobiska, Improved space weather observations and modeling for aviation radiation, Front. Astron. Space Sci. 10 (2023) 1149014.
[57] C.J. Mertens, W.K. Tobiska, Space weather radiation effects on high-altitude/-latitude aircraft, Space Weather Eff. Appl. (2021) 79–110.
[58] D. Xue, J. Yang, Z. Liu, B. Wang, An optimized solution to long-distance flight routes under extreme cosmic radiation, Space Weather (2022) e2022SW003264.
[59] D. Xue, L. Wu, T. Xu, C.L. Wu, Z. Wang, Z. He, Space weather effects on transportation systems: a review of current understanding and future outlook, Space Weather 22 (12) (2024) e2024SW004055.